
Segment, Shuffle, and Stitch: A Simple Mechanism for Improving Time-Series Representations

Shivam Grover, Amin Jalali, Ali Etemad

Queen's University, Canada

{shivam.grover, amin.jalali, ali.etemad}@queensu.ca

Abstract

Existing approaches for learning representations of time-series keep the temporal arrangement of the time-steps intact with the presumption that the original order is the most optimal for learning. However, non-adjacent sections of real-world time-series may have strong dependencies. Accordingly we raise the question: *Is there an alternative arrangement for time-series which could enable more effective representation learning?* To address this, we propose a simple plug-and-play mechanism called Segment, Shuffle, and Stitch (S3) designed to improve time-series representation learning of existing models. S3 works by creating non-overlapping segments from the original sequence and shuffling them in a learned manner that is the most optimal for the task at hand. It then re-attaches the shuffled segments back together and performs a learned weighted sum with the original input to capture both the newly shuffled sequence along with the original sequence. S3 is modular and can be stacked to create various degrees of granularity, and can be added to many forms of neural architectures including CNNs or Transformers with negligible computation overhead. Through extensive experiments on several datasets and state-of-the-art baselines, we show that incorporating S3 results in significant improvements for the tasks of time-series classification and forecasting, improving performance on certain datasets by up to 68%. We also show that S3 makes the learning more stable with a smoother training loss curve and loss landscape compared to the original baseline. The code is available at <https://github.com/shivam-grover/S3-TimeSeries>.

1 Introduction

Time-series data serve an important role across diverse domains, including but not limited to health analytics [1, 2, 3], human-computer interaction [4, 5], climate analysis [6, 7], energy consumption [8, 9, 10], traffic management [11, 12], financial markets [13, 14], and others. The pervasive nature of time-series data has resulted in considerable interest among researchers, leading to the development of a variety of deep learning solutions for classification [15, 16, 17] and forecasting [8, 18, 19, 20]. Neural architectures such as convolutional networks [15, 21], recurrent networks [22, 23], and Transformers [8, 19] can capture the essential spatial and temporal information from time-series. Notably, these approaches have frequently outperformed traditional approaches, including Dynamic Time Warping [24], Bag of Stochastic Frontier Analysis Symbols [25], and the Collective of Transformation-Based Ensembles [26] in various scenarios.

While both traditional machine learning and deep learning solutions aim to extract effective goal-related representations prior to classification or forecasting, the general approach is to keep the original temporal arrangement of the time-steps in the time-series intact, with the presumption that the original order is the most optimal. Moreover, most existing models do not have explicit mechanisms to explore the inter-relations between distant segments within each time-series, which may in fact

have strong dependencies despite their lack of proximity. For example, CNN-based models for time-series learning generally utilize fixed convolutional filters and receptive fields, causing them to only capture patterns within a limited temporal window [27, 28]. As a result, when faced with time-series where important patterns or correlations span across longer time windows, these models will struggle to capture this information effectively [28]. Dilated convolutional neural networks partially solve this by increasing the receptive field through the dilation rate. However, they are still practically limited by their inherent architectures, as their receptive fields rely on the number of layers, which may not be large enough to fully capture the long-range dependencies and can lead to vanishing gradients as more layers are added [29]. Similarly, the out-of-the-box effectiveness of Transformers [30] in capturing long-term dependencies highly depends on a variety of factors such as sequence length, positional encoding, and tokenization strategies. Accordingly, we ask a simple question: *Is there a better arrangement for the time-series that would enable more effective representation learning considering the classification/forecasting task at hand?*

In this paper, we introduce a simple and plug-and-play mechanism called **Segment, Shuffle, and Stitch**, or **S3** for short, designed to enhance time-series representation learning. As the name suggests, S3 operates by segmenting the time-series into several segments, shuffling these segments in the most optimal order controlled by learned shuffling parameters, and then stitching the shuffled segments. In addition to this, our module integrates the original time-series through a learned weighted sum operation with the shuffled version to also preserve the key information in the original order. S3 acts as a modular mechanism intended to seamlessly integrate with any time-series model and as we will demonstrate experimentally, results in a smoother training procedure and loss landscape. Since S3 is trained along with the backbone network, the shuffling parameter is updated in a goal-centric manner, adapting to the characteristics of the data and the backbone model to better capture the temporal dynamics. Finally, S3 can be stacked to create a more fine-grained shuffling with higher levels of granularity, has very few hyper-parameters to tune, and has negligible computation overhead.

For evaluation, we integrate S3 in a variety of neural architectures including CNN-based and Transformer-based models, and evaluate performance across various classification, univariate forecasting, and multivariate forecasting datasets, observing that S3 results in substantial improvements when integrated into state-of-the-art (SOTA) models. Specifically, the results demonstrate that integrating S3 into state-of-the-art methods can improve performance by up to 39.59% for classification, and by up to 68.71% and 51.22% for univariate and multivariate forecasting, respectively. We perform detailed ablation and sensitivity studies to analyze different components of our proposed S3 layer.

Our contributions are summarized as follows.

- We propose S3, a simple and modular mechanism that can be plugged into existing neural architectures to improve time-series representation learning. By dynamically segmenting and shuffling the input time-series across the temporal dimension, S3 helps the model perform more effective task-centric representation learning.
- By stacking multiple instances of S3, the model can perform shuffling at different granularity levels. Our proposed layer has very few hyperparameters and negligible added computational cost.
- Rigorous experiments on various benchmark time-series datasets across both classification and forecasting tasks demonstrate that by incorporating S3 into existing state-of-the-art baselines, we improve performance significantly. Experiments also show that by adding our proposed mechanism, more stable training is achieved.
- We make our code public to contribute to the field of time-series representation learning and enable fast and accurate reproducibility.

2 Related work

Deep learning architectures have recently made significant progress in the area of time-series representation learning. In the category of **convolution-based** methods, T-Loss [31] uses causal dilated convolutions and time-based negative sampling using a triplet-loss for obtaining representations. DSN [15] introduces dynamic sparse connections to cover different receptive fields in convolution layers for time-series classification. In another convolution-based approach, SCINet [21] captures temporal

features by partitioning each time sequence into two subsequences at each level to effectively model the complex temporal dynamics within hierarchical time-series data.

Transformer-based approaches are another category of solutions which have drawn considerable attention. Informer [8] improves the capabilities of the vanilla Transformer on long input sequences by introducing self-attention distillation using ProbSparse which is based on Kullback-Leibler divergence, and a generative style decoder. Autoformer [19] introduces decomposition blocks with an auto-correlation mechanism which allows progressive decomposition of the data. ContiFormer [32] integrates the continuous dynamics of Neural Ordinary Differential Equations with the attention mechanism of Transformers. Finally, [33] investigated the effectiveness of Transformers in dealing with long sequences for forecasting and highlighted the challenges Transformers encounter in this regard.

Contrastive methods have recently demonstrated SOTA performances in time-series learning. TNC [34] generates neighborhoods within the time-series and uses a debiased contrastive objective to distinguish the neighboring distribution of signals from the non-neighboring signals. TS2Vec [16] employs unsupervised hierarchical contrastive learning across augmented contextual views, capturing robust representations at various semantic levels. InfoTS [35] uses information-aware augmentations for contrastive learning which dynamically chooses the optimal augmentations. TF-C [36] contrasts representations across both time and frequency domains to learn time-series representations. To address long-term forecasting, [28] introduces a contrastive approach that incorporates global autocorrelation alongside a decomposition network. Finally, SoftCLT [37] is a recent contrastive approach that uses the distances between time-series samples (instance-wise contrastive) along with the difference in timestamps (temporal contrastive), to capture the correlations between adjacent samples and improved representations.

Given the existence of seasonal and trend information in time-series, **disentanglement** is an approach that has been widely used across both classical machine learning [38, 39, 40] and deep learning solutions [41, 18]. For instance, CoST [41] attempts to capture periodic patterns using frequency domain contrastive loss to disentangle seasonal-trend representations in both time and frequency domains. Similarly, LaST [18] recently employed variational inference to learn and disentangle latent seasonal and trend components within time-series data.

3 Method

Problem definition. Given a set of N time-series instances as $\{\mathbf{x}_i\}_{i=1}^N$, where $\mathbf{x}_i \in \mathbb{R}^{T \times C}$ has a length of T and C channels, the goal is to optimally rearrange the segments of \mathbf{x}_i and form a new sequence \mathbf{x}'_i to better capture the underlying temporal relationships and dependencies within the time-series, which would consequently lead to improved representations given the target task.

Proposed mechanism. We propose S3, a simple neural network component for addressing the aforementioned problem in three steps, as the name suggests, Segment, Shuffle, and Stitch, described below (see Figure 1).

The Segment module splits the input sequence \mathbf{x}_i into n non-overlapping segments, each containing τ time-steps, where $\tau = T/n$. The set of segments can be represented by $\mathbf{S}_i = \{\mathbf{s}_{i,1}, \mathbf{s}_{i,2}, \dots, \mathbf{s}_{i,n}\} \in \mathbb{R}^{(\tau \times C) \times n}$ where $\mathbf{s}_{i,j} = \mathbf{x}_i[(j-1)\tau : j\tau]$ and $\mathbf{s}_{i,j} \in \mathbb{R}^{\tau \times C}$.

The segments are then fed into the Shuffle module, which uses a shuffle vector $\mathbf{P} = \{p_1, p_2, \dots, p_n\} \in \mathbb{R}^n$ to rearrange the seg-

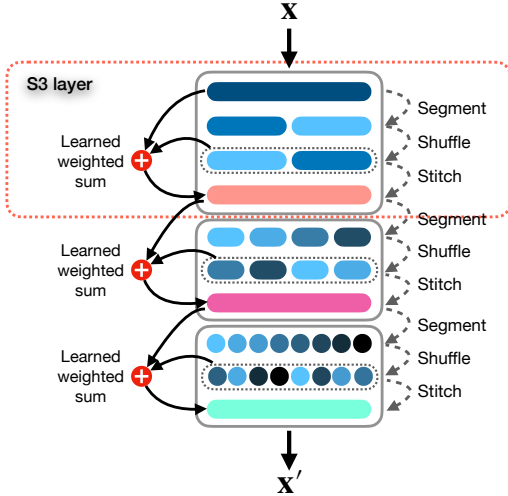


Figure 1: Stacking S3 layers. In this depiction, we use $n = 2$, $\phi = 3$, and $\theta = 2$ as the hyperparameters.

ments in the optimal order for the task at hand. Each shuffling parameter p_j in \mathbf{P} corresponds to a segment $s_{i,j}$ in \mathbf{S}_i . \mathbf{P} is essentially a set of learnable weights optimized through the network’s learning process, which controls the position and priority of the segment in the reordered sequence. The shuffling process is quite simple and intuitive: the higher the value of p_j , the higher the priority of segment $s_{i,j}$ is in the shuffled sequence. The shuffled sequence $\mathbf{S}_i^{\text{shuffled}}$ can be represented as

$$\mathbf{S}_i^{\text{shuffled}} = \text{Sort}(\mathbf{S}_i, \text{key} = \mathbf{P}), \quad (1)$$

where the segments in \mathbf{S}_i are sorted according to the values in \mathbf{P} . Permuting \mathbf{S}_i based on the sorted order of \mathbf{P} is not differentiable by default, because it involves discrete operations and introduces discontinuities [42]. Soft sorting methods such as [43, 42, 44] approximate the sorted order by assigning probabilities that reflect how much larger each element is compared to others. While this approximation is differentiable in nature, it may introduce noise and inaccuracies, while making the sorting non-intuitive. To achieve differentiable sorting and permutation that are as accurate and intuitive as traditional methods, we introduce a few intermediate steps. These steps create a path for gradients to flow through the shuffling parameters \mathbf{P} while performing discrete permutations on \mathbf{S}_i based on the sorted order of \mathbf{P} . We first obtain the indices that sort the elements of \mathbf{P} using $\sigma = \text{Argsort}(\mathbf{P})$. We have a list of tensors $\mathbf{S} = [s_1, s_2, s_3, \dots, s_n]$ (for simplicity, we skip the index i) that we aim to reorder based on the list of indices $\sigma = [\sigma_1, \sigma_2, \dots, \sigma_n]$ in a differentiable way. We then create a $(\tau \times C) \times n \times n$ matrix \mathbf{U} , which we populate by repeating each s_i , n times. Next, we form an $n \times n$ matrix $\mathbf{\Omega}$ where each row j has a single non-zero element at position $k = \sigma_j$ which is p_k . We convert $\mathbf{\Omega}$ to a binary matrix $\tilde{\mathbf{\Omega}}$ by scaling each non-zero element to 1 using a scaling factor $\frac{1}{\Omega_{j,k}}$. This process creates a path for the gradients to flow through \mathbf{P} during backpropagation.

By performing the Hadamard product between \mathbf{U} and $\tilde{\mathbf{\Omega}}$, we obtain a matrix \mathbf{V} where each row j has one non-zero element k equals to s_k . Finally, by summing along the final dimension and transposing the outcome, we obtain the final shuffled matrix of size $\mathbf{S}_i^{\text{shuffled}} \in \mathbb{R}^{\tau \times C \times n}$. To better illustrate, we show a simple example with $\mathbf{S} = [s_1, s_2, s_3, s_4]$ and a given permutation $\sigma = [3, 4, 1, 2]$. We calculate \mathbf{V} as

$$\mathbf{V} = \mathbf{U} \odot \tilde{\mathbf{\Omega}} = \begin{bmatrix} s_1 & s_2 & s_3 & s_4 \\ s_1 & s_2 & s_3 & s_4 \\ s_1 & s_2 & s_3 & s_4 \\ s_1 & s_2 & s_3 & s_4 \end{bmatrix} \odot \begin{bmatrix} 0 & 0 & 1 & 0 \\ 0 & 0 & 0 & 1 \\ 1 & 0 & 0 & 0 \\ 0 & 1 & 0 & 0 \end{bmatrix} = \begin{bmatrix} 0 & 0 & s_3 & 0 \\ 0 & 0 & 0 & s_4 \\ s_1 & 0 & 0 & 0 \\ 0 & s_2 & 0 & 0 \end{bmatrix}, \quad (2)$$

and $\mathbf{S}_i^{\text{shuffled}}$ is obtained by

$$\mathbf{S}_i^{\text{shuffled}} = \left(\sum_{k=1}^n (\mathbf{V}_{j,k}) \right)^T = [s_3 \quad s_4 \quad s_1 \quad s_2]. \quad (3)$$

We previously assumed that the set of shuffling parameters \mathbf{P} is one-dimensional, containing n scalar elements, each corresponding to one of the segments. By employing a higher-dimensional \mathbf{P} , we can introduce additional parameters that enable the model to capture complex representations that a single-dimensional \mathbf{P} could struggle with. Therefore, we introduce a hyperparameter λ to determine the dimensionality of the vector \mathbf{P} . When $\lambda = m$, the size of \mathbf{P} becomes $n \times n \times \dots \times n$ (repeated m times). We then perform a summation of \mathbf{P} over the first $m - 1$ dimensions to obtain a one-dimensional vector. Mathematically, this is represented as

$$\tilde{\mathbf{P}} = \sum_{d_1=1}^n \sum_{d_2=1}^n \dots \sum_{d_{m-1}=1}^n \mathbf{P}_{d_1, d_2, \dots, d_{m-1}}. \quad (4)$$

This results in a one-dimensional matrix $\tilde{\mathbf{P}}$, which we then use to compute the permutation indices $\sigma = \text{Argsort}(\tilde{\mathbf{P}})$. This approach allows us to increase the number of shuffling parameters, thereby capturing more complex dependencies within the time-series data, without affecting the sorting operations.

In the final step, the `Stitch` module concatenates the shuffled segments $\mathbf{S}_i^{\text{shuffled}}$ to create a single shuffled sequence $\tilde{\mathbf{x}}_i \in \mathbb{R}^{T \times C}$ as $\tilde{\mathbf{x}}_i = \text{Concat}(\mathbf{S}_i^{\text{shuffled}})$. To retain the information present in the original order along with the newly generated shuffled sequence, we perform a weighted sum between \mathbf{x}_i and $\tilde{\mathbf{x}}_i$ with learnable weights \mathbf{w}_1 and \mathbf{w}_2 optimized through the training of the main network.

For practical convenience, we can use a simple learnable Conv1D or MLP layer taking \mathbf{x}_i and $\tilde{\mathbf{x}}_i$ as inputs and generating the final time-series output $\mathbf{x}'_i \in \mathbb{R}^{T \times C}$.

Stacking S3 layers. Considering S3 as a modular layer, we can stack them sequentially within a neural architecture. Let’s define ϕ as a hyperparameter that determines the number of S3 layers. For simplicity and to avoid defining a separate segment hyperparameter for each S3 layer, we define θ which acts as a multiplier for the number of segments in subsequent layers as

$$n_\ell = n \times \theta^{\ell-1} \quad \text{for } \ell = 1, 2, \dots, \phi, \quad (5)$$

where n is the number of segments in the first S3 layer. When multiple S3 layers are stacked, each layer ℓ from 1 to ϕ will segment and shuffle its input based on the output from the previous layer. We can formally represent the output of each layer ℓ as \mathbf{x}'_ℓ by

$$\mathbf{x}'_\ell = \text{Stitch}(\text{Shuffle}(\text{Segment}(\mathbf{x}'_{\ell-1}, n_\ell), \mathbf{P}_\ell), (\mathbf{w}_{\ell,1}, \mathbf{w}_{\ell,2})), \text{ for } \ell = 1, 2, \dots, \phi, \quad (6)$$

where \mathbf{x}'_0 is the original time-series \mathbf{x} , \mathbf{P}_ℓ is the set of shuffling parameters for layer ℓ , and $(\mathbf{w}_{\ell,1}, \mathbf{w}_{\ell,2})$ are the learnable weights for the sum operation between the concatenation of the shuffled segments and the original input, at layer ℓ . Figure 1 presents an example of three S3 layers ($\phi = 3$) applied to a time-series with $n = 2$ and $\theta = 2$.

All the \mathbf{P}_ℓ values are updated along with the model parameters, and there is no intermediate loss for any of the S3 layers. This ensures that the S3 layers are trained according to the specific task and the baseline. In cases where the length of input sequence \mathbf{x} is not divisible by the number of segments n , we resort to truncating the first $T \bmod n$ time-steps from the input sequence. In order to ensure that no data is lost and the input and output shapes are the same, we later add the truncated samples back at the beginning of the output of the final S3 layer.

4 Experiment setup

Evaluation protocol. For our experiments, we integrate S3 into existing SOTA models for both time-series classification and forecasting. We first train and evaluate each model adhering strictly to their original setups and experimental protocols. We then integrate S3 at the beginning of the model, and train and evaluate it with the exact same setups and protocols as the original models. This meticulous approach ensures that any observed deviation in performance can be fairly attributed to the integration of S3. For classification, we measure the percentage improvement in accuracy resulting from S3 as $(Acc_{\text{Baseline+S3}} - Acc_{\text{Baseline}}) / Acc_{\text{Baseline}}$. For forecasting, since lower MSE is better, we use $(MSE_{\text{Baseline}} - MSE_{\text{Baseline+S3}}) / MSE_{\text{Baseline}}$ to measure the percentage of improvement in MSE. A similar equation is used for the percentage of improvement in MAE.

Classification datasets. For classification we use the following datasets: (1) The **UCR archive** [45] which consists of 128 univariate datasets, (2) the **UEA archive** [46] which consists of 30 multivariate datasets, and (3) three multivariate datasets namely **EEG**, **EEG2**, and **HAR** from the UCI archive [47]. The train/test split for all 3 classification datasets are as provided in the original papers.

Forecasting datasets. For forecasting, we use both the univariate and multivariate versions of three **ETT** datasets [8]: **ETT_{h1}** and **ETT_{h2}** recorded hourly, and **ETT_{m1}** recorded at every 15 minutes. The train/val/test split is 12/4/4 months following [8].

Baselines. We select baselines from a variety of different time-series learning approaches including CNN-based, Transformer-based, contrastive, and disentanglement. Specifically, for classification, we use four state-of-the-art baseline methods, SoftCLT [37], TS2Vec [16], DSN [15], and InfoTS [35]. For forecasting, we use three state-of-the-art baseline methods, TS2Vec [16], LaST [18], and Informer [8]. We incorporate one to three layers of S3 into the input level of each baseline and compare the performance of the modified model with the original model.

Implementation details. All implementation details match those of the baselines. We used the exact hyperparameters of the baselines according to the original papers when they were specified in the papers or the code was available; alternatively, when the hyperparameters were not exactly specified in the paper or in the code, we tried to maximize performance with our own search for the optimum hyperparameters. Accordingly, **some baseline results may slightly differ from those available in the original papers.** Note that deviations in baseline results affect both the baseline model and baseline + S3. For the weighted sum operation in S3, we use Conv1D. Our code is implemented with Pytorch, and our experiments are conducted on a single Nvidia Quadro RTX 6000 GPU. We release the code at: <https://github.com/shivam-grover/S3-TimeSeries>.

5 Results

Classification. The results of our experiments on time-series classification are presented in Table 1. In this table we observe the addition of S3 results in substantial improvements across all baselines for all univariate and multivariate datasets. For UCR, UEA, EEG, EEG2, and HAR, we achieve average improvements of 3.89%, 5.25%, 32.03%, 9.675%, and 5.18% respectively over all models. The full classification results on UCR and UEA datasets for all baselines with and without S3 are mentioned in Appendix (Table A1 and A2). These results highlight the efficacy of S3 in improving a variety of different classification methods over a diverse set of datasets despite negligible added computational complexity (we provide a detailed discussion on computation overhead later in this section). In addition to quantitative metrics, we also visualise the t-SNE plots for several datasets in Figure 2 and Appendix A1, which show that adding S3 results in representations with better class separability in the latent space.

Table 1: Comparison with baselines on time-series classification

| Method | UCR | UEA | EEG | EEG2 | HAR |
|-------------|--------------|--------------|--------------|--------------|--------------|
| TS2Vec | 0.819 | 0.695 | 0.593 | 0.845 | 0.930 |
| TS2Vec+S3 | 0.851 | 0.720 | 0.672 | 0.9733 | 0.935 |
| Improvement | 3.90% | 3.63% | 19.47% | 15.18% | 11.31% |
| DSN | 0.794 | 0.687 | 0.516 | 0.961 | 0.957 |
| DSN+S3 | 0.833 | 0.736 | 0.717 | 0.980 | 0.971 |
| Improvement | 4.85% | 7.24% | 38.90% | 1.93% | 1.41% |
| InfoTS | 0.733 | 0.691 | 0.515 | 0.822 | 0.876 |
| InfoTS+S3 | 0.760 | 0.727 | 0.719 | 0.947 | 0.929 |
| Improvement | 3.71% | 5.34% | 39.59% | 15.21% | 6.05% |
| SoftCLT | 0.825 | 0.699 | 0.516 | 0.893 | 0.918 |
| SoftCLT+S3 | 0.845 | 0.734 | 0.672 | 0.950 | 0.936 |
| Improvement | 2.42% | 4.76% | 30.16% | 6.38% | 1.96% |

Forecasting. Table 2 presents a comprehensive overview of the results for univariate forecasting on different datasets and horizons (H), with and without the incorporation of S3. We observe that S3 consistently leads to improvements for all baseline methods across all datasets, with an average improvement in MSE and MAE of 5.82% and 4.49% for TS2Vec, 5.16% and 3.72% for LaST, and 21.37% and 10.02% for informer. Figure 3 shows two forecasting outputs for Informer with and without S3, on two different horizon lengths for a sample from the ETTh1 dataset. In both cases, S3 improves the ability of the baseline Informer to generate time-series samples that better align

Table 2: Univariate forecasting results for different baselines with and without S3.

| Dataset | H | Metric | TS2Vec | TS2Vec+S3 | Improvement | LaST | LaST+S3 | Improvement | Informer | Informer+S3 | Improvement | |
|---------|---------|--------|---------------|---------------|-------------|--------|---------------|---------------|----------|---------------|-------------|-------|
| ETTh1 | 24 | MSE | 0.0409 | 0.0370 | 9.40% | 0.0295 | 0.0293 | 0.80% | 0.1169 | 0.0851 | 27.18% | |
| | | MAE | 0.1614 | 0.1459 | 9.58% | 0.1297 | 0.1291 | 0.45% | 0.2753 | 0.2263 | 17.76% | |
| | 48 | MSE | 0.0714 | 0.0605 | 15.24% | 0.0479 | 0.0464 | 3.07% | 0.1358 | 0.1132 | 16.57% | |
| | | MAE | 0.2035 | 0.1884 | 7.45% | 0.1630 | 0.1628 | 0.11% | 0.2959 | 0.2727 | 7.81% | |
| | 168 | MSE | 0.1362 | 0.1202 | 11.71% | 0.0765 | 0.0731 | 4.40% | 0.1604 | 0.0944 | 41.12% | |
| | | MAE | 0.3235 | 0.2663 | 17.65% | 0.2071 | 0.2069 | 0.10% | 0.3207 | 0.2434 | 24.10% | |
| | 336 | MSE | 0.1699 | 0.1426 | 16.09% | 0.0948 | 0.0920 | 2.89% | 0.1411 | 0.1021 | 27.59% | |
| | | MAE | 0.3333 | 0.2949 | 11.54% | 0.2409 | 0.2366 | 1.80% | 0.2990 | 0.2532 | 15.30% | |
| | 720 | MSE | 0.1739 | 0.1734 | 0.29% | 0.1417 | 0.1370 | 3.33% | 0.269 | 0.0841 | 68.71% | |
| | | MAE | 0.3307 | 0.3359 | -1.58% | 0.3098 | 0.2989 | 3.50% | 0.2159 | 0.1980 | 8.27% | |
| | ETTh2 | 24 | MSE | 0.0973 | 0.0938 | 3.49% | 0.0708 | 0.0675 | 4.58% | 0.0851 | 0.0844 | 0.75% |
| | | | MAE | 0.2363 | 0.2344 | 0.82% | 0.1956 | 0.1902 | 3.20% | 0.2230 | 0.2210 | 1.02% |
| 48 | | MSE | 0.1269 | 0.1242 | 1.77% | 0.0995 | 0.0939 | 5.72% | 0.1503 | 0.1461 | 2.77% | |
| | | MAE | 0.2781 | 0.2761 | 0.72% | 0.2394 | 0.2279 | 4.80% | 0.3036 | 0.2990 | 1.54% | |
| 168 | | MSE | 0.1974 | 0.1853 | 6.12% | 0.1796 | 0.1680 | 6.40% | 0.2637 | 0.2470 | 6.34% | |
| | | MAE | 0.3562 | 0.3437 | 3.50% | 0.3194 | 0.3098 | 3.02% | 0.4120 | 0.3756 | 8.83% | |
| 336 | | MSE | 0.2031 | 0.1953 | 3.86% | 0.2213 | 0.2049 | 7.39% | 0.3177 | 0.2993 | 5.79% | |
| | | MAE | 0.3638 | 0.3551 | 2.41% | 0.3819 | 0.3579 | 6.28% | 0.4543 | 0.4432 | 2.44% | |
| 720 | | MSE | 0.2084 | 0.1983 | 4.82% | 0.2754 | 0.2712 | 1.53% | 0.2678 | 0.2548 | 4.88% | |
| | | MAE | 0.3719 | 0.3620 | 2.36% | 0.4297 | 0.4215 | 1.91% | 0.4199 | 0.3975 | 5.34% | |
| ETTm1 | | 24 | MSE | 0.0150 | 0.0152 | -1.74% | 0.0231 | 0.0229 | 16.22% | 0.0246 | 0.0228 | 7.13% |
| | | | MAE | 0.0910 | 0.0928 | -1.96% | 0.1070 | 0.0982 | 8.25% | 0.1117 | 0.1079 | 3.33% |
| | 48 | MSE | 0.0283 | 0.0290 | -2.44% | 0.0479 | 0.0465 | 3.08% | 0.0561 | 0.0501 | 10.76% | |
| | | MAE | 0.1304 | 0.1350 | -3.52% | 0.1580 | 0.1517 | 3.99% | 0.1749 | 0.1632 | 6.70% | |
| | 96 | MSE | 0.0480 | 0.0458 | 4.41% | 0.0765 | 0.0715 | 6.53% | 0.1124 | 0.1100 | 2.15% | |
| | | MAE | 0.1713 | 0.1643 | 4.07% | 0.2071 | 0.1967 | 5.04% | 0.2421 | 0.2433 | -0.51% | |
| | 228 | MSE | 0.0992 | 0.0953 | 3.92% | 0.1058 | 0.0953 | 9.94% | 0.1833 | 0.1762 | 3.87% | |
| | | MAE | 0.2495 | 0.2359 | 5.46% | 0.2490 | 0.2231 | 10.40% | 0.3368 | 0.3209 | 4.73% | |
| | 672 | MSE | 0.1568 | 0.1529 | 2.50% | 0.1699 | 0.1589 | 6.47% | 0.2686 | 0.2582 | 3.88% | |
| | | MAE | 0.3100 | 0.3028 | 2.33% | 0.3165 | 0.3089 | 2.75% | 0.4212 | 0.4166 | 1.10% | |
| | Average | MSE | 0.1182 | 0.1115 | 5.82% | 1.1110 | 1.1053 | 5.16% | 0.1702 | 0.1338 | 21.37% | |
| | | MAE | 0.2607 | 0.2490 | 4.49% | 0.2437 | 0.2346 | 3.72% | 0.3005 | 0.2704 | 10.02% | |

Table 3: Multivariate forecasting results for different baselines with and without S3

| Dataset | H | Metric | TS2Vec | TS2Vec+S3 | Improvement | LaST | LaST+S3 | Improvement | Informer | Informer+S3 | Improvement |
|---------|-----|--------|--------|-----------|-------------|---------------|---------------|-------------|---------------|-------------|-------------|
| ETTh1 | 24 | MSE | 0.5360 | 0.5048 | 5.82% | 0.3230 | 0.3249 | -0.55% | 0.5344 | 0.4928 | 7.79% |
| | | MAE | 0.5026 | 0.4866 | 3.19% | 0.3632 | 0.3654 | -0.61% | 0.5253 | 0.4939 | 5.97% |
| | 48 | MSE | 0.5907 | 0.5596 | 5.27% | 0.3804 | 0.3513 | 7.65% | 0.7471 | 0.6738 | 9.80% |
| | | MAE | 0.5499 | 0.5160 | 6.17% | 0.4064 | 0.3792 | 6.69% | 0.6621 | 0.6228 | 5.92% |
| | 168 | MSE | 0.7498 | 0.7016 | 6.43% | 0.5149 | 0.4633 | 10.02% | 1.0853 | 0.9689 | 10.72% |
| | | MAE | 0.6350 | 0.6011 | 6.43% | 0.4906 | 0.4497 | 8.32% | 0.8307 | 0.7828 | 5.77% |
| | 336 | MSE | 0.8841 | 0.8631 | 2.38% | 0.7102 | 0.5828 | 17.93% | 1.3561 | 1.0734 | 20.84% |
| | | MAE | 0.7049 | 0.6856 | 2.74% | 0.6182 | 0.5308 | 14.10% | 0.9550 | 0.8339 | 6.61% |
| | 720 | MSE | 1.0471 | 1.0441 | 0.30% | 0.9354 | 0.7765 | 16.98% | 1.3860 | 1.2597 | 9.11% |
| | | MAE | 0.7884 | 0.7798 | 1.09% | 0.7470 | 0.6652 | 11.00% | 0.9575 | 0.9031 | 5.87% |
| ETTh2 | 24 | MSE | 0.4106 | 0.3516 | 14.37% | 0.1760 | 0.1745 | 0.83% | 0.3865 | 0.3696 | 4.38% |
| | | MAE | 0.4786 | 0.4352 | 9.07% | 0.2679 | 0.2667 | 0.46% | 0.4753 | 0.4578 | 3.68% |
| | 48 | MSE | 0.5969 | 0.5355 | 10.28% | 0.2663 | 0.2242 | 15.80% | 2.4910 | 2.1537 | 13.54% |
| | | MAE | 0.5952 | 0.5533 | 7.04% | 0.3084 | 0.3018 | 2.11% | 1.2874 | 1.1683 | 9.25% |
| | 168 | MSE | 1.8673 | 1.6609 | 11.05% | 0.7635 | 0.6992 | 8.42% | 4.9837 | 2.8678 | 42.46% |
| | | MAE | 1.0730 | 0.9924 | 7.52% | 0.6082 | 0.5757 | 5.35% | 1.9106 | 1.4202 | 25.67% |
| | 336 | MSE | 2.3067 | 1.7424 | 24.47% | 1.2567 | 1.0107 | 19.58% | 3.0175 | 3.1162 | -3.27% |
| | | MAE | 1.2217 | 1.3067 | 15.14% | 0.7978 | 0.7095 | 11.06% | 1.4438 | 1.4891 | -3.84% |
| | 720 | MSE | 2.7273 | 2.2901 | 16.03% | 1.1952 | 1.7197 | 11.92% | 4.3677 | 3.3177 | 24.04% |
| | | MAE | 1.4042 | 1.2268 | 12.64% | 1.1171 | 1.0620 | 4.93% | 1.8087 | 1.5454 | 14.56% |
| ETTm1 | 24 | MSE | 0.5388 | 0.3959 | 26.52% | 0.1036 | 0.1002 | 3.19% | 0.9264 | 0.4995 | 46.08% |
| | | MAE | 0.4958 | 0.4297 | 13.33% | 0.2098 | 0.2039 | 2.78% | 0.7183 | 0.5401 | 24.81% |
| | 48 | MSE | 0.6498 | 0.4748 | 26.93% | 0.1386 | 0.1331 | 3.92% | 0.2599 | 0.2313 | 11.02% |
| | | MAE | 0.5580 | 0.4698 | 15.84% | 0.2428 | 0.2358 | 2.86% | 0.3732 | 0.3550 | 4.86% |
| | 96 | MSE | 0.6439 | 0.5194 | 19.33% | 0.1823 | 0.1822 | 0.03% | 1.7790 | 1.4871 | 16.41% |
| | | MAE | 0.5677 | 0.5043 | 11.17% | 0.2726 | 0.2714 | 0.41% | 1.0455 | 0.9602 | 8.16% |
| | 228 | MSE | 0.7224 | 0.6149 | 14.87% | 0.3062 | 0.2823 | 7.82% | 6.2431 | 3.0455 | 51.22% |
| | | MAE | 0.6231 | 0.5645 | 9.40% | 0.3665 | 0.3477 | 5.13% | 2.1601 | 1.4082 | 34.80% |
| | 672 | MSE | 0.7530 | 0.6810 | 9.56% | 0.9525 | 0.8908 | 6.47% | 7.3624 | 6.3159 | 14.21% |
| | | MAE | 0.6418 | 0.6056 | 5.65% | 0.7232 | 0.6546 | 9.47% | 2.4195 | 2.1142 | 12.62% |
| Average | MSE | 1.0017 | 0.8627 | 13.87% | 0.5975 | 0.5278 | 11.67% | 2.4618 | 1.8582 | 24.52% | |
| | MAE | 0.7227 | 0.6596 | 8.73% | 0.5027 | 0.4680 | 6.89% | 1.1709 | 1.0062 | 14.06% | |

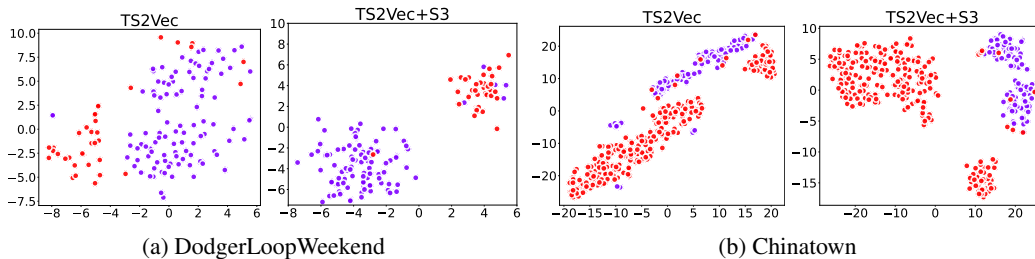


Figure 2: t-SNE visualizations of the learned representations of TS2Vec and TS2Vec+S3 for 4 randomly chosen test sets. Different colors represent different classes. It can be seen that representations belonging to different classes are more separable after adding S3.

with the ground truth. Similarly, Table 3 presents the results of multivariate forecasting. Consistent with univariate forecasting, S3 significantly enhances the performance of the baseline on multivariate forecasting and achieves average improvements in MSE and MAE of 13.87% and 8.73% for TS2Vec, 11.67% and 6.89% for LaST, and 24.52% and 14.06% for Informer.

Loss behaviour. We make interesting observations while training the baseline models as well as the baseline+S3 variants. First, we observe that the training loss vs. epochs for baseline+S3 variants generally converge faster than the original baselines. See Figure 4 where we demonstrate examples of this behavior. Second, we observe that the training loss curves for baseline+S3 are generally much smoother than the original baselines. This can again be observed in Figure 4. Additionally, we measure the standard deviations of the loss curves for SoftCLT with and without S3 on all the UCR datasets and measure an average reduction in standard deviation of 36.66%. The detailed values for the standard deviations of the loss curves are presented in Appendix A3. Lastly, according to [48], we investigate the loss landscape of the baselines and observe that the addition of S3 generally results in a smoother loss landscape with fewer local minima (Figure 5). Additional examples are provided in Appendix A2.

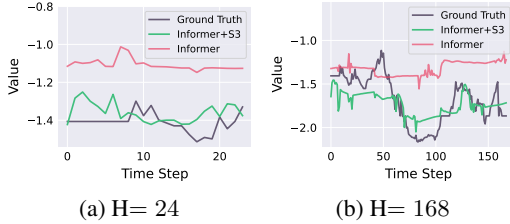


Figure 3: Forecasting output by Informer and Informer+S3 for a sample from ETTh1.

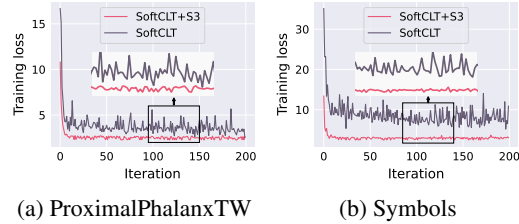


Figure 4: Training loss against iterations on two sample datasets from the UCR archive.

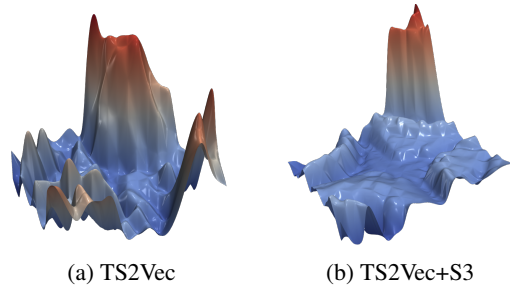


Figure 5: Visualisation of the loss landscape for the Beef dataset from the UCR archive.

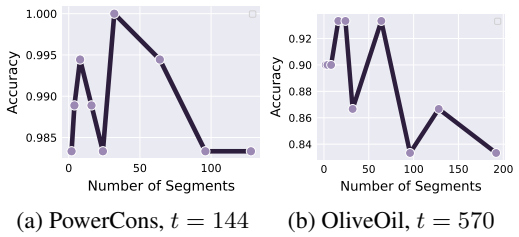


Figure 6: Classification accuracy vs. number of segments for two sample datasets from UCR with different input sequence lengths t .

Ablation. We perform ablation studies to investigate the impact of each of the key modules of S3 and answer three questions: **(1)** Do we need the *Segment* module to divide the input into multiple segments, or will shuffling all the time-steps individually work just as well? **(2)** Do we need learned *Shuffling* parameters (**P**) to determine the optimal permutation of the time series, or will random permutations work just as well? **(3)** Do we need the *Stitch* module to apply a learned weighted sum of the original sequence with the shuffled sequence, or will the shuffled sequences alone work just as well? Table 5 shows the results of three ablation studies where we observe that the removal of each component of S3 results in a decline in performance.

Hyperparameters. Next, we investigate the impact of the number of segments n on performance. Considering all the experiments, we observe that no general rule of thumb can be advised for n , as its optimum value is naturally highly dependant on factors such as dataset complexity, length, baselines, and others. We present two examples in Figure 6 and more in Appendix A3 where we plot the accuracy vs. number of segments for datasets of different lengths from UCR. As for the other hyperparameters, the number of S3 layers ϕ has been set between 1, 2, or 3 across all of the experiments in this paper. θ , the multiple for the number of segments in stacked S3 layers, has been set to 0.5, 1, or 2 across all our experiments. And finally λ has only been set to 1, 2, or 3. The ranges of values for all the hyperparameters used in this work are presented in Table 4. While optimizing hyperparameters is important, similar to any other form of representation learning, we find that even sub-optimal tuning of S3 hyperparameters still yields meaningful improvements. We perform a simple experiment where we apply a uniform set of hyperparameters [$n = 2, \phi = 2, \theta = 1, \lambda = 1$] to all the baselines and baselines with added S3 layers. The results for this experiment are presented in Table 6 where we observe that despite not using the optimum hyperparameters, the addition of S3 still yields considerable performance boosts. The optimum hyperparameters used for each experiment are made available in the code.

Table 4: Range of hyperparameters.

| | Range |
|-----------|---------------------|
| n | [2, 4, 8, 16, 24] |
| ϕ | [1, 2, 3] |
| θ | [0.5, 1, 2] |
| λ | [1, 2, 3] |

Sensitivity to random seed. To evaluate the impact of the random seed on the performance of S3, we perform 10 separate trials with different seed values and present the standard deviations in Table 7. The first 4 rows show the classification baselines trained on the UCI datasets with and without S3. Similarly, the next 3 rows show forecasting baselines trained on the multivariate ETTh1 dataset (H=24) with and without S3. From this experiment, we observe that the addition of S3 has not considerable impact on the sensitivity of the original baselines to the random seed.

Shuffling parameters. In Figure 7, we present a visual overview of how the parameters of **P** update along with the parent model during training on ETTh1 (H=48) and ETTm1 (H=48). Each parameter

Table 5: **Ablation** results for classification.

| Method | EEG | EEG2 | HAR |
|------------------------|-------|-------|-------|
| TS2Vec+S3 | 0.672 | 0.973 | 0.935 |
| TS2Vec+S3 w/o Segment | 0.552 | 0.872 | 0.865 |
| TS2Vec+S3 w/o P | 0.562 | 0.864 | 0.906 |
| TS2Vec+S3 w/o Stitch | 0.584 | 0.871 | 0.901 |
| DSN+S3 | 0.717 | 0.980 | 0.971 |
| DSN+S3 w/o Segment | 0.516 | 0.929 | 0.910 |
| DSN+S3 w/o P | 0.490 | 0.953 | 0.828 |
| DSN+S3 w/o Stitch | 0.550 | 0.934 | 0.856 |
| InfoTS+S3 | 0.719 | 0.947 | 0.929 |
| InfoTS+S3 w/o Segment | 0.535 | 0.865 | 0.898 |
| InfoTS+S3 w/o P | 0.499 | 0.845 | 0.869 |
| InfoTS+S3 w/o Stitch | 0.515 | 0.821 | 0.887 |
| SoftCLT+S3 | 0.672 | 0.950 | 0.936 |
| SoftCLT+S3 w/o Segment | 0.548 | 0.919 | 0.879 |
| SoftCLT+S3 w/o P | 0.523 | 0.905 | 0.883 |
| SoftCLT+S3 w/o Stitch | 0.600 | 0.913 | 0.921 |

Table 6: Classification results with **common hyperparameters**.

| Method | EEG | EEG2 | HAR |
|-------------|--------|--------|--------|
| TS2Vec | 0.593 | 0.845 | 0.926 |
| TS2Vec+S3 | 0.625 | 0.910 | 0.922 |
| Improvement | 11.11% | 7.69% | -0.36% |
| DSN | 0.516 | 0.961 | 0.957 |
| DSN+S3 | 0.567 | 0.978 | 0.974 |
| Improvement | 9.83% | 1.78% | 1.72% |
| InfoTS | 0.515 | 0.822 | 0.876 |
| InfoTS+S3 | 0.593 | 0.842 | 0.898 |
| Improvement | 15.15% | 2.43% | 2.45% |
| SoftCLT | 0.500 | 0.893 | 0.918 |
| SoftCLT+S3 | 0.640 | 0.890 | 0.923 |
| Improvement | 15.15% | -0.33% | 0.54% |

Table 7: Variation to **seed**.

| Method | w/o S3 | w/ S3 |
|---------|--------|--------|
| SoftCLT | 0.0044 | 0.0058 |
| TS2Vec | 0.0077 | 0.0075 |
| InfoTS | 0.0067 | 0.0082 |
| DSN | 0.0041 | 0.0035 |
| TS2Vec | 0.0019 | 0.0028 |
| Informr | 0.0144 | 0.0142 |
| LaST | 0.0009 | 0.0012 |

Table 8: **Parameter count**.

| Method | Baseline | S3 |
|---------|----------|-----|
| TS2Vec | 613k | 24 |
| SoftCLT | 641k | 579 |
| InfoTS | 606k | 7 |
| DSN | 106k | 13 |
| TS2Vec | 638k | 12 |
| Informr | 11.3M | 6 |
| LaST | 130k | 16 |

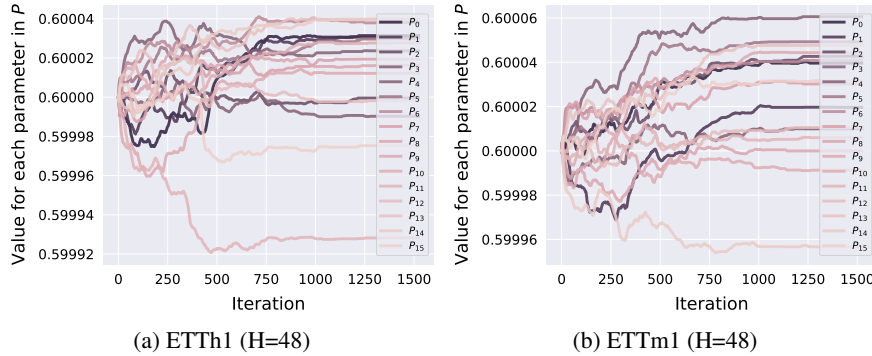


Figure 7: The progression of the shuffling parameters during training for LaST+S3.

in \mathbf{P} corresponds to a segment of \mathbf{S} . In both cases, we set n to 16 and ϕ to 1. The baseline used is LaST [18]. It can be seen that the individual weights in \mathbf{P} rearrange the corresponding segments until they reach a stable point (the optimal order) after which the order of the segments is maintained.

Computation overhead. Our proposed mechanism adds very few learnable parameters to the baseline models, which stem from a learnable shuffling vector \mathbf{P} along with \mathbf{w}_1 and \mathbf{w}_2 , per each S3 layer. To emphasize the negligible computation overhead of S3 in comparison to the baseline models, we show the total number of parameters in the baseline and the total learnable parameters that S3 adds, in Table 8 for classification on the EEG2 dataset and forecasting on the multivariate ETTh1 dataset (H=24).

6 Conclusion

Summary. We propose S3, a simple plug-and-play neural network component that rearranges the time series in three steps: **S**egment the time series, **S**huffle the segments, and **S**titch the shuffled time-series by concatenating the segments and performing a learned sum with the original time-series. Through extensive experiments on time-series classification and forecasting with state-of-the-art methods, we show that S3 improves the learning capabilities of the baseline with negligible computation overhead. We also show empirically that S3 helps in faster and smoother training leading to better performance.

Limitations. While we present the effectiveness of S3 on a diverse set of baselines on classification and forecasting tasks, we acknowledge that the evaluation on other time-series tasks such as imputation and anomaly detection remain for future work. Additionally applying S3 to learning videos is an interesting direction for future research.

Broader impact. Since S3 is a plug-and-play mechanism with negligible added parameters, it allows researchers from various domains related to time-series such as health signal processing, biometrics, climate analysis, financial markets, and others to use this module in their existing models without the need for redesign. The low computation overhead also makes S3 a suitable choice for edge-devices.

References

- [1] Rajat Doshi, Yunyang Li, Garrett I. Ash, Jason Liu, Laura Nally, Matthew A Stults-Kolehmainen, Stuart A Weinzimer, Lisa M. Fucito, and Mark Gerstein. Forecasting exercise lapses in individuals with type 1 diabetes using state space models. In *ICLR Workshop on Learning from Time Series For Health*, 2024. [1](#)
- [2] Aniruddh Raghu, Payal Chandak, Ridwan Alam, John Guttag, and Collin Stultz. Contrastive pre-training for multimodal medical time series. In *NeurIPS Workshop on Learning from Time Series for Health*, 2022. [1](#)
- [3] Satya Narayan Shukla and Benjamin Marlin. Multi-time attention networks for irregularly sampled time series. In *International Conference on Learning Representations*, 2021. [1](#)
- [4] Zekai Chen, Xiao Zhang, and Xiuzhen Cheng. Asm2tv: an adaptive semi-supervised multi-task multi-view learning framework for human activity recognition. In *AAAI Conference on Artificial Intelligence*, volume 36, pages 6342–6349, 2022. [1](#)
- [5] Luay Alawneh, Tamam Alsarhan, Mohammad Al-Zinati, Mahmoud Al-Ayyoub, Yaser Jararweh, and Hongtao Lu. Enhancing human activity recognition using deep learning and time series augmented data. *Journal of Ambient Intelligence and Humanized Computing*, pages 1–16, 2021. [1](#)
- [6] Sijie He, Xinyan Li, Timothy DelSole, Pradeep Ravikumar, and Arindam Banerjee. Sub-seasonal climate forecasting via machine learning: Challenges, analysis, and advances. In *AAAI Conference on Artificial Intelligence*, volume 35, pages 169–177, 2021. [1](#)
- [7] Haitao Lin, Zhangyang Gao, Yongjie Xu, Lirong Wu, Ling Li, and Stan Z Li. Conditional local convolution for spatio-temporal meteorological forecasting. In *AAAI Conference on Artificial Intelligence*, volume 36, pages 7470–7478, 2022. [1](#)
- [8] Haoyi Zhou, Shanghang Zhang, Jieqi Peng, Shuai Zhang, Jianxin Li, Hui Xiong, and Wancai Zhang. Informer: Beyond efficient transformer for long sequence time-series forecasting. In *AAAI Conference on Artificial Intelligence*, volume 35, pages 11106–11115, 2021. [1](#), [3](#), [5](#)
- [9] Seok-Jun Bu and Sung-Bae Cho. Time series forecasting with multi-headed attention-based deep learning for residential energy consumption. *Energies*, 13(18):4722, 2020. [1](#)
- [10] Zhiyuan Wang, Xovee Xu, Goce Trajcevski, Kunpeng Zhang, Ting Zhong, and Fan Zhou. Pref: Probabilistic electricity forecasting via copula-augmented state space model. In *AAAI Conference on Artificial Intelligence*, volume 36, pages 12200–12207, 2022. [1](#)
- [11] Lei Bai, Lina Yao, Can Li, Xianzhi Wang, and Can Wang. Adaptive graph convolutional recurrent network for traffic forecasting. *Advances in Neural Information Processing Systems*, 33:17804–17815, 2020. [1](#)
- [12] Razvan-Gabriel Cirstea, Bin Yang, Chenjuan Guo, Tung Kieu, and Shirui Pan. Towards spatio-temporal aware traffic time series forecasting. In *IEEE International Conference on Data Engineering*, pages 2900–2913, 2022. [1](#)
- [13] Dawei Cheng, Fangzhou Yang, Sheng Xiang, and Jin Liu. Financial time series forecasting with multi-modality graph neural network. *Pattern Recognition*, 121:108218, 2022. [1](#)
- [14] Milena Vuletić, Felix Prenzel, and Mihai Cucuringu. Fin-gan: Forecasting and classifying financial time series via generative adversarial networks. *Quantitative Finance*, pages 1–25, 2024. [1](#)
- [15] Qiao Xiao, Boqian Wu, Yu Zhang, Shiwei Liu, Mykola Pechenizkiy, Elena Mocanu, and Decebal Constantin Mocanu. Dynamic sparse network for time series classification: Learning what to “see”. *Advances in Neural Information Processing Systems*, 35:16849–16862, 2022. [1](#), [2](#), [5](#)
- [16] Zhihan Yue, Yujing Wang, Juanyong Duan, Tianmeng Yang, Congrui Huang, Yunhai Tong, and Bixiong Xu. Ts2vec: Towards universal representation of time series. In *AAAI Conference on Artificial Intelligence*, volume 36, pages 8980–8987, 2022. [1](#), [3](#), [5](#)
- [17] Xuchao Zhang, Yifeng Gao, Jessica Lin, and Chang-Tien Lu. Tapnet: Multivariate time series classification with attentional prototypical network. In *AAAI Conference on Artificial Intelligence*, volume 34, pages 6845–6852, 2020. [1](#)

- [18] Zhiyuan Wang, Xovee Xu, Weifeng Zhang, Goce Trajcevski, Ting Zhong, and Fan Zhou. Learning latent seasonal-trend representations for time series forecasting. *Advances in Neural Information Processing Systems*, 35:38775–38787, 2022. 1, 3, 5, 9
- [19] Haixu Wu, Jiehui Xu, Jianmin Wang, and Mingsheng Long. Autoformer: Decomposition transformers with auto-correlation for long-term series forecasting. *Advances in Neural Information Processing Systems*, 34:22419–22430, 2021. 1, 3
- [20] Ricardo P Masini, Marcelo C Medeiros, and Eduardo F Mendes. Machine learning advances for time series forecasting. *Journal of Economic Surveys*, 37(1):76–111, 2023. 1
- [21] Minhao Liu, Ailing Zeng, Muxi Chen, Zhijian Xu, Qiuxia Lai, Lingna Ma, and Qiang Xu. Scinet: Time series modeling and forecasting with sample convolution and interaction. *Advances in Neural Information Processing Systems*, 35:5816–5828, 2022. 1, 2
- [22] Qingxiong Tan, Mang Ye, Baoyao Yang, Siqi Liu, Andy Jinhua Ma, Terry Cheuk-Fung Yip, Grace Lai-Hung Wong, and PongChi Yuen. Data-gru: Dual-attention time-aware gated recurrent unit for irregular multivariate time series. In *AAAI Conference on Artificial Intelligence*, volume 34, pages 930–937, 2020. 1
- [23] Donghui Chen, Ling Chen, Youdong Zhang, Bo Wen, and Chenghu Yang. A multiscale interactive recurrent network for time-series forecasting. *IEEE Transactions on Cybernetics*, 52(9):8793–8803, 2021. 1
- [24] Hassan Ismail Fawaz, Germain Forestier, Jonathan Weber, Lhassane Idoumghar, and Pierre-Alain Muller. Deep learning for time series classification: a review. *Data Mining and Knowledge Discovery*, 33(4):917–963, 2019. 1
- [25] Patrick Schäfer. The boss is concerned with time series classification in the presence of noise. *Data Mining and Knowledge Discovery*, 29:1505–1530, 2015. 1
- [26] Anthony Bagnall, Jason Lines, Jon Hills, and Aaron Bostrom. Time-series classification with cote: the collective of transformation-based ensembles. *IEEE Transactions on Knowledge and Data Engineering*, 27(9):2522–2535, 2015. 1
- [27] Aosong Feng and Leandros Tassioulas. Adaptive graph spatial-temporal transformer network for traffic forecasting. In *ACM International Conference on Information and Knowledge Management*, pages 3933–3937, 2022. 2
- [28] Junwoo Park, Daehoon Gwak, Jaegul Choo, and Edward Choi. Self-supervised contrastive learning for long-term forecasting. In *International Conference on Learning Representations*, 2024. 2, 3
- [29] Ali Salehi and Madhusudhanan Balasubramanian. Ddcnet: Deep dilated convolutional neural network for dense prediction. *Neurocomputing*, 523:116–129, 2023. 2
- [30] Ashish Vaswani, Noam Shazeer, Niki Parmar, Jakob Uszkoreit, Llion Jones, Aidan N Gomez, Łukasz Kaiser, and Illia Polosukhin. Attention is all you need. *Advances in Neural Information Processing Systems*, 30, 2017. 2
- [31] Jean-Yves Franceschi, Aymeric Dieuleveut, and Martin Jaggi. Unsupervised scalable representation learning for multivariate time series. *Advances in Neural Information Processing Systems*, 32, 2019. 2
- [32] Yuqi Chen, Kan Ren, Yansen Wang, Yuchen Fang, Weiwei Sun, and Dongsheng Li. Contiformer: Continuous-time transformer for irregular time series modeling. *Advances in Neural Information Processing Systems*, 36, 2024. 3
- [33] Ailing Zeng, Muxi Chen, Lei Zhang, and Qiang Xu. Are transformers effective for time series forecasting? In *AAAI Conference on Artificial Intelligence*, volume 37, pages 11121–11128, 2023. 3
- [34] Sana Tonekaboni, Danny Eytan, and Anna Goldenberg. Unsupervised representation learning for time series with temporal neighborhood coding. In *International Conference on Learning Representations*, 2020. 3
- [35] Dongsheng Luo, Wei Cheng, Yingheng Wang, Dongkuan Xu, Jingchao Ni, Wenchao Yu, Xuchao Zhang, Yanchi Liu, Yuncong Chen, Haifeng Chen, et al. Time series contrastive learning with information-aware augmentations. In *AAAI Conference on Artificial Intelligence*, volume 37, pages 4534–4542, 2023. 3, 5

- [36] Kexin Zhang, Qingsong Wen, Chaoli Zhang, Rongyao Cai, Ming Jin, Yong Liu, James Y Zhang, Yuxuan Liang, Guansong Pang, Dongjin Song, et al. Self-supervised learning for time series analysis: Taxonomy, progress, and prospects. *IEEE Transactions on Pattern Analysis and Machine Intelligence*, 2024. 3
- [37] Seunghan Lee, Taeyoung Park, and Kibok Lee. Soft contrastive learning for time series. In *The International Conference on Learning Representations*, 2024. 3, 5
- [38] Renfei He, Limao Zhang, and Alvin Wei Ze Chew. Modeling and predicting rainfall time series using seasonal-trend decomposition and machine learning. *Knowledge-Based Systems*, 251:109125, 2022. 3
- [39] Robert B Cleveland, William S Cleveland, Jean E McRae, Irma Terpenning, et al. STI: A seasonal-trend decomposition. *Journal of Official Statistics*, 6(1):3–73, 1990. 3
- [40] Shuai Liu, Xiucheng Li, Gao Cong, Yile Chen, and Yue Jiang. Multivariate time-series imputation with disentangled temporal representations. In *International Conference on Learning Representations*, 2022. 3
- [41] Gerald Woo, Chenghao Liu, Doyen Sahoo, Akshat Kumar, and Steven Hoi. CoST: Contrastive learning of disentangled seasonal-trend representations for time series forecasting. In *International Conference on Learning Representations*, 2022. 3
- [42] Marco Cuturi, Olivier Teboul, and Jean-Philippe Vert. Differentiable ranking and sorting using optimal transport. *Advances in Neural Information Processing Systems*, 32, 2019. 4
- [43] Mathieu Blondel, Olivier Teboul, Quentin Berthet, and Josip Djolonga. Fast differentiable sorting and ranking. In *International Conference on Machine Learning*, pages 950–959, 2020. 4
- [44] Michael Taylor, John Guiver, Stephen Robertson, and Tom Minka. Softrank: optimizing non-smooth rank metrics. In *International Conference on Web Search and Data Mining*, pages 77–86, 2008. 4
- [45] Hoang Anh Dau, Anthony Bagnall, Kaveh Kamgar, Chin-Chia Michael Yeh, Yan Zhu, Shaghayegh Gharghabi, Chotirat Ann Ratanamahatana, and Eamonn Keogh. The ucr time series archive. *IEEE Journal of Automatica Sinica*, 6(6):1293–1305, 2019. 5
- [46] Anthony Bagnall, Hoang Anh Dau, Jason Lines, Michael Flynn, James Large, Aaron Bostrom, Paul Southam, and Eamonn Keogh. The uea multivariate time series classification archive, 2018. *ArXiv Preprint arXiv:1811.00075*, 2018. 5
- [47] Dheeru Dua and Casey Graff. Welcome to the uc irvine machine learning repository, 2017. 5
- [48] Hao Li, Zheng Xu, Gavin Taylor, Christoph Studer, and Tom Goldstein. Visualizing the loss landscape of neural nets. *Advances in Neural Information Processing Systems*, 31, 2018. 7, 15

A Appendix

A.1 Additional results

We show the full results for all baselines with and without S3 on 128 UCR datasets in Table A1 and on 30 UEA datasets in Table A2. In Figure A1 we show 2 more t-SNE plots for TS2Vec trained on 2 randomly chosen UCR datasets. A better clustering of different classes can be observed in the learned representations after S3 is incorporated. In Table A3 we compare the standard deviation values for the training loss of SoftCLT and SoftCLT+S3. From this figure we observe that after incorporating S3, the training becomes much more stable with significantly less variations. Figure A2 shows 2 more comparisons of the loss landscape of TS2Vec trained with and without S3. In Figure A3 we present 6 more samples for the impact of n on the performance of the model.

Table A1: Per-dataset breakdown of results for the UCR archive.

| Dataset | TS2Vec | TS2Vec+S3 | DSN | DSN+S3 | InfoTS | InfoTS+S3 | SoftCLT | SoftCLT+S3 |
|------------------------------|--------------|--------------|--------------|--------------|--------------|--------------|--------------|--------------|
| ACSF1 | 0.778 | 0.830 | 0.790 | 0.810 | 0.800 | 0.800 | 0.800 | 0.860 |
| Adiac | 0.737 | 0.785 | 0.767 | 0.859 | 0.703 | 0.621 | 0.772 | 0.795 |
| AllGestureWiimoteX | 0.773 | 0.790 | 0.710 | 0.753 | 0.117 | 0.211 | 0.743 | 0.794 |
| AllGestureWiimoteY | 0.779 | 0.797 | 0.704 | 0.797 | 0.146 | 0.406 | 0.777 | 0.786 |
| AllGestureWiimoteZ | 0.723 | 0.773 | 0.744 | 0.753 | 0.160 | 0.203 | 0.740 | 0.746 |
| ArrowHead | 0.834 | 0.886 | 0.800 | 0.926 | 0.846 | 0.851 | 0.823 | 0.863 |
| BME | 0.987 | 1.000 | 0.827 | 0.950 | 0.993 | 1.000 | 1.000 | 1.000 |
| Beef | 0.700 | 0.967 | 0.433 | 0.500 | 0.700 | 0.833 | 0.733 | 0.967 |
| BeetleFly | 0.900 | 0.950 | 0.800 | 0.950 | 0.800 | 0.950 | 0.850 | 0.900 |
| BirdChicken | 0.800 | 1.000 | 0.900 | 1.000 | 0.750 | 0.900 | 0.800 | 1.000 |
| CBF | 1.000 | 1.000 | 0.968 | 1.000 | 1.000 | 1.000 | 0.968 | 0.999 |
| Car | 0.733 | 0.900 | 0.900 | 0.933 | 0.717 | 0.750 | 0.767 | 0.900 |
| Chinatown | 0.965 | 0.991 | 0.959 | 0.980 | 0.971 | 0.977 | 0.980 | 0.985 |
| ChlorineConcentration | 0.815 | 0.836 | 0.833 | 0.894 | 0.754 | 0.750 | 0.754 | 0.820 |
| CinCECGTorso | 0.817 | 0.935 | 0.796 | 0.981 | 0.801 | 0.857 | 0.824 | 0.954 |
| Coffee | 1.000 | 1.000 | 1.000 | 1.000 | 0.964 | 1.000 | 1.000 | 1.000 |
| Computers | 0.628 | 0.680 | 0.800 | 0.808 | 0.664 | 0.660 | 0.640 | 0.688 |
| CricketX | 0.795 | 0.808 | 0.800 | 0.828 | 0.700 | 0.718 | 0.785 | 0.810 |
| CricketY | 0.764 | 0.785 | 0.808 | 0.836 | 0.733 | 0.721 | 0.769 | 0.756 |
| CricketZ | 0.800 | 0.805 | 0.831 | 0.828 | 0.751 | 0.715 | 0.790 | 0.808 |
| Crop | 0.755 | 0.758 | 0.740 | 0.730 | 0.752 | 0.750 | 0.761 | 0.759 |
| DiatomSizeReduction | 0.984 | 0.997 | 0.915 | 0.997 | 0.961 | 0.990 | 0.974 | 0.990 |
| DistalPhalanxOutlineAgeGroup | 0.727 | 0.770 | 0.788 | 0.845 | 0.741 | 0.741 | 0.748 | 0.755 |
| DistalPhalanxOutlineCorrect | 0.732 | 0.793 | 0.772 | 0.833 | 0.757 | 0.772 | 0.728 | 0.797 |
| DistalPhalanxTW | 0.676 | 0.719 | 0.750 | 0.790 | 0.683 | 0.727 | 0.676 | 0.705 |
| DodgerLoopDay | 0.563 | 0.650 | 0.413 | 0.435 | 0.625 | 0.513 | 0.500 | 0.575 |
| DodgerLoopGame | 0.848 | 0.920 | 0.768 | 0.779 | 0.783 | 0.797 | 0.862 | 0.877 |
| DodgerLoopWeekend | 0.964 | 0.986 | 0.986 | 0.986 | 0.978 | 0.971 | 0.949 | 0.986 |
| Earthquakes | 0.748 | 0.748 | 0.710 | 0.829 | 0.748 | 0.770 | 0.748 | 0.748 |
| ECG200 | 0.910 | 0.960 | 0.840 | 0.930 | 0.880 | 0.890 | 0.890 | 0.950 |
| ECG5000 | 0.933 | 0.940 | 0.945 | 0.944 | 0.941 | 0.942 | 0.939 | 0.943 |
| ECGFiveDays | 1.000 | 1.000 | 0.986 | 1.000 | 0.866 | 0.984 | 1.000 | 1.000 |
| ElectricDevices | 0.519 | 0.724 | 0.723 | 0.723 | 0.723 | 0.684 | 0.711 | 0.709 |
| EOGHorizontalSignal | 0.503 | 0.514 | 0.503 | 0.583 | 0.500 | 0.544 | 0.561 | 0.564 |
| EOGVerticalSignal | 0.500 | 0.508 | 0.412 | 0.497 | 0.525 | 0.539 | 0.525 | 0.525 |
| EthanolLevel | 0.420 | 0.626 | 0.644 | 0.676 | 0.306 | 0.630 | 0.658 | 0.659 |
| FaceAll | 0.768 | 0.818 | 0.792 | 0.789 | 0.756 | 0.769 | 0.820 | 0.823 |
| FaceFour | 0.852 | 0.841 | 0.966 | 0.966 | 0.920 | 0.943 | 0.932 | 0.875 |
| FacesUCR | 0.926 | 0.947 | 0.965 | 0.979 | 0.893 | 0.873 | 0.940 | 0.935 |
| FiftyWords | 0.771 | 0.815 | 0.826 | 0.822 | 0.767 | 0.763 | 0.793 | 0.809 |
| Fish | 0.931 | 0.931 | 0.989 | 0.967 | 0.800 | 0.840 | 0.937 | 0.846 |
| FordA | 0.935 | 0.933 | 0.947 | 0.954 | 0.815 | 0.801 | 0.917 | 0.926 |
| FordB | 0.796 | 0.806 | 0.933 | 0.940 | 0.606 | 0.673 | 0.788 | 0.795 |
| FreezerRegularTrain | 0.985 | 0.990 | 0.996 | 0.991 | 0.982 | 0.981 | 0.991 | 0.996 |
| FreezerSmallTrain | 0.868 | 0.941 | 0.796 | 0.928 | 0.740 | 0.781 | 0.972 | 0.981 |
| Fungi | 0.957 | 0.968 | 1.000 | 1.000 | 1.000 | 1.000 | 0.973 | 0.957 |
| GestureMidAirD1 | 0.615 | 0.715 | 0.638 | 0.746 | 0.077 | 0.092 | 0.723 | 0.700 |
| GestureMidAirD2 | 0.469 | 0.608 | 0.577 | 0.610 | 0.085 | 0.092 | 0.562 | 0.615 |
| GestureMidAirD3 | 0.308 | 0.431 | 0.300 | 0.423 | 0.077 | 0.108 | 0.392 | 0.477 |
| GesturePebbleZ1 | 0.907 | 0.872 | 0.837 | 0.924 | 0.314 | 0.238 | 0.913 | 0.872 |
| GesturePebbleZ2 | 0.848 | 0.892 | 0.778 | 0.804 | 0.310 | 0.437 | 0.861 | 0.892 |
| GunPoint | 0.980 | 0.993 | 0.993 | 0.993 | 0.980 | 0.987 | 0.993 | 0.993 |
| GunPointAgeSpan | 0.965 | 0.994 | 0.981 | 1.000 | 0.956 | 0.978 | 0.956 | 1.000 |
| GunPointMaleVersusFemale | 1.000 | 1.000 | 0.997 | 1.000 | 1.000 | 1.000 | 1.000 | 1.000 |
| GunPointOldVersusYoung | 1.000 | 1.000 | 1.000 | 1.000 | 1.000 | 1.000 | 1.000 | 1.000 |
| Ham | 0.733 | 0.810 | 0.752 | 0.790 | 0.781 | 0.638 | 0.771 | 0.819 |
| HandOutlines | 0.924 | 0.919 | 0.852 | 0.848 | 0.908 | 0.916 | 0.850 | 0.849 |
| Haptics | 0.516 | 0.545 | 0.565 | 0.594 | 0.403 | 0.438 | 0.503 | 0.512 |
| Herring | 0.594 | 0.688 | 0.672 | 0.734 | 0.578 | 0.594 | 0.641 | 0.688 |
| HouseTwenty | 0.908 | 0.966 | 0.924 | 0.983 | 0.891 | 0.874 | 0.933 | 0.941 |
| InlineSkate | 0.407 | 0.420 | 0.431 | 0.480 | 0.333 | 0.345 | 0.429 | 0.402 |
| InsectEPGRegularTrain | 1.000 | 1.000 | 1.000 | 1.000 | 1.000 | 1.000 | 1.000 | 1.000 |
| InsectEPGSmallTrain | 1.000 | 1.000 | 0.474 | 1.000 | 1.000 | 1.000 | 1.000 | 1.000 |
| InsectWingbeatSound | 0.634 | 0.641 | 0.581 | 0.636 | 0.647 | 0.637 | 0.625 | 0.638 |
| ItalyPowerDemand | 0.924 | 0.971 | 0.959 | 0.965 | 0.945 | 0.965 | 0.964 | 0.972 |

Continued on next page

Table A1 – continued from previous page

| Dataset | TS2Vec | TS2Vec+S3 | DSN | DSN+S3 | InfoTS | InfoTS+S3 | SoftCLT | SoftCLT+S3 |
|--------------------------------|--------------|--------------|--------------|--------------|--------------|--------------|--------------|--------------|
| LargeKitchenAppliances | 0.867 | 0.864 | 0.880 | 0.928 | 0.821 | 0.827 | 0.827 | 0.867 |
| Lightning2 | 0.852 | 0.885 | 0.770 | 0.803 | 0.721 | 0.787 | 0.836 | 0.852 |
| Lightning7 | 0.849 | 0.836 | 0.808 | 0.890 | 0.822 | 0.849 | 0.822 | 0.808 |
| Mallat | 0.922 | 0.940 | 0.961 | 0.972 | 0.912 | 0.944 | 0.915 | 0.946 |
| Meat | 0.950 | 1.000 | 0.867 | 0.950 | 0.933 | 0.917 | 0.950 | 0.983 |
| MedicalImages | 0.788 | 0.801 | 0.753 | 0.770 | 0.770 | 0.745 | 0.793 | 0.792 |
| MelbournePedestrian | 0.957 | 0.961 | 0.948 | 0.949 | 0.945 | 0.946 | 0.961 | 0.963 |
| MiddlePhalanxOutlineAgeGroup | 0.636 | 0.656 | 0.720 | 0.790 | 0.649 | 0.649 | 0.630 | 0.675 |
| MiddlePhalanxOutlineCorrect | 0.818 | 0.821 | 0.793 | 0.828 | 0.735 | 0.759 | 0.821 | 0.838 |
| MiddlePhalanxTW | 0.571 | 0.623 | 0.581 | 0.639 | 0.610 | 0.610 | 0.578 | 0.610 |
| MixedShapesRegularTrain | 0.920 | 0.926 | 0.977 | 0.983 | 0.916 | 0.920 | 0.925 | 0.939 |
| MixedShapesSmallTrain | 0.846 | 0.882 | 0.939 | 0.950 | 0.856 | 0.877 | 0.894 | 0.884 |
| Motestrain | 0.858 | 0.884 | 0.907 | 0.851 | 0.885 | 0.882 | 0.874 | 0.876 |
| NonInvasiveFetalECGThorax1 | 0.928 | 0.944 | 0.926 | 0.926 | 0.904 | 0.904 | 0.933 | 0.937 |
| NonInvasiveFetalECGThorax2 | 0.932 | 0.948 | 0.916 | 0.892 | 0.926 | 0.913 | 0.946 | 0.965 |
| OliveOil | 0.900 | 0.933 | 0.467 | 0.967 | 0.867 | 0.933 | 0.833 | 0.856 |
| OSULeaf | 0.851 | 0.839 | 0.979 | 0.992 | 0.603 | 0.612 | 0.818 | 0.831 |
| PhalangesOutlinesCorrect | 0.793 | 0.817 | 0.832 | 0.837 | 0.801 | 0.800 | 0.801 | 0.825 |
| Phoneme | 0.304 | 0.298 | 0.325 | 0.341 | 0.197 | 0.319 | 0.299 | 0.304 |
| PickupGestureWiimoteZ | 0.820 | 0.840 | 0.820 | 0.843 | 0.320 | 0.400 | 0.880 | 0.900 |
| PigAirwayPressure | 0.644 | 0.663 | 0.471 | 0.889 | 0.139 | 0.163 | 0.332 | 0.361 |
| PigArtPressure | 0.966 | 0.962 | 0.320 | 0.284 | 0.337 | 0.418 | 0.966 | 0.962 |
| PigCVP | 0.793 | 0.817 | 0.269 | 0.254 | 0.139 | 0.188 | 0.832 | 0.798 |
| PLAID | 0.553 | 0.547 | 0.214 | 0.203 | 0.067 | 0.179 | 0.512 | 0.538 |
| Plane | 0.990 | 1.000 | 1.000 | 1.000 | 0.981 | 0.981 | 0.981 | 1.000 |
| PowerCons | 0.961 | 1.000 | 0.928 | 0.967 | 0.989 | 0.994 | 0.994 | 0.994 |
| ProximalPhalanxOutlineAgeGroup | 0.829 | 0.868 | 0.868 | 0.878 | 0.859 | 0.859 | 0.854 | 0.863 |
| ProximalPhalanxOutlineCorrect | 0.883 | 0.900 | 0.911 | 0.924 | 0.845 | 0.873 | 0.869 | 0.911 |
| ProximalPhalanxTW | 0.800 | 0.829 | 0.828 | 0.825 | 0.790 | 0.824 | 0.824 | 0.820 |
| RefrigerationDevices | 0.589 | 0.608 | 0.528 | 0.584 | 0.579 | 0.571 | 0.603 | 0.584 |
| Rock | 0.740 | 0.740 | 0.500 | 0.600 | 0.500 | 0.700 | 0.857 | 0.740 |
| ScreenType | 0.416 | 0.448 | 0.597 | 0.645 | 0.440 | 0.469 | 0.453 | 0.445 |
| SemgHandGenderCh2 | 0.947 | 0.948 | 0.618 | 0.574 | 0.937 | 0.963 | 0.937 | 0.958 |
| SemgHandMovementCh2 | 0.862 | 0.876 | 0.431 | 0.436 | 0.831 | 0.858 | 0.841 | 0.864 |
| SemgHandSubjectCh2 | 0.951 | 0.920 | 0.656 | 0.456 | 0.869 | 0.929 | 0.947 | 0.936 |
| ShakeGestureWiimoteZ | 0.940 | 0.960 | 0.940 | 0.914 | 0.400 | 0.600 | 0.920 | 0.960 |
| ShapeletSim | 0.989 | 1.000 | 0.767 | 0.872 | 0.528 | 0.600 | 1.000 | 0.994 |
| ShapesAll | 0.903 | 0.905 | 0.903 | 0.905 | 0.780 | 0.808 | 0.898 | 0.893 |
| SmallKitchenAppliances | 0.733 | 0.733 | 0.821 | 0.835 | 0.739 | 0.731 | 0.712 | 0.752 |
| SmoothSubspace | 0.980 | 0.987 | 0.947 | 0.912 | 0.987 | 0.940 | 0.993 | 0.980 |
| SonyAIBORobotSurface1 | 0.890 | 0.930 | 0.965 | 0.972 | 0.839 | 0.895 | 0.884 | 0.864 |
| SonyAIBORobotSurface2 | 0.872 | 0.923 | 0.929 | 0.892 | 0.794 | 0.851 | 0.876 | 0.813 |
| StarLightCurves | 0.968 | 0.939 | 0.981 | 0.983 | 0.959 | 0.960 | 0.968 | 0.965 |
| Strawberry | 0.962 | 0.968 | 0.972 | 0.984 | 0.957 | 0.962 | 0.954 | 0.962 |
| SwedishLeaf | 0.939 | 0.938 | 0.979 | 0.981 | 0.936 | 0.934 | 0.947 | 0.938 |
| Symbols | 0.973 | 0.948 | 0.927 | 0.922 | 0.939 | 0.946 | 0.960 | 0.967 |
| SyntheticControl | 0.993 | 0.993 | 0.993 | 0.997 | 0.980 | 0.987 | 0.997 | 0.993 |
| ToeSegmentation1 | 0.934 | 0.912 | 0.974 | 0.978 | 0.741 | 0.825 | 0.934 | 0.952 |
| ToeSegmentation2 | 0.900 | 0.900 | 0.946 | 0.962 | 0.846 | 0.900 | 0.877 | 0.938 |
| Trace | 1.000 | 1.000 | 1.000 | 1.000 | 1.000 | 1.000 | 1.000 | 1.000 |
| TwoLeadECG | 0.987 | 0.990 | 0.996 | 0.999 | 0.753 | 0.910 | 0.977 | 0.994 |
| TwoPatterns | 1.000 | 0.994 | 0.949 | 1.000 | 0.999 | 1.000 | 1.000 | 1.000 |
| UMD | 0.993 | 1.000 | 0.979 | 0.934 | 1.000 | 1.000 | 1.000 | 1.000 |
| UWaveGestureLibraryAll | 0.929 | 0.956 | 0.902 | 0.906 | 0.959 | 0.963 | 0.950 | 0.970 |
| UWaveGestureLibraryX | 0.790 | 0.817 | 0.833 | 0.833 | 0.806 | 0.824 | 0.829 | 0.811 |
| UWaveGestureLibraryY | 0.719 | 0.739 | 0.771 | 0.776 | 0.723 | 0.730 | 0.736 | 0.746 |
| UWaveGestureLibraryZ | 0.764 | 0.780 | 0.784 | 0.788 | 0.732 | 0.754 | 0.772 | 0.769 |
| Wafer | 0.996 | 0.997 | 0.992 | 0.999 | 0.989 | 0.996 | 0.999 | 0.998 |
| Wine | 0.870 | 0.944 | 0.556 | 0.722 | 0.759 | 0.815 | 0.519 | 0.981 |
| WordSynonyms | 0.680 | 0.708 | 0.724 | 0.732 | 0.687 | 0.687 | 0.701 | 0.718 |
| Worms | 0.649 | 0.805 | 0.619 | 0.663 | 0.649 | 0.610 | 0.714 | 0.779 |
| WormsTwoClass | 0.701 | 0.870 | 0.751 | 0.779 | 0.597 | 0.727 | 0.766 | 0.818 |
| Yoga | 0.872 | 0.885 | 0.882 | 0.919 | 0.829 | 0.841 | 0.881 | 0.890 |
| Average | 0.819 | 0.851 | 0.794 | 0.833 | 0.733 | 0.760 | 0.825 | 0.845 |

Table A2: Per-dataset breakdown of classification results for the UEA dataset.

| Dataset | TS2Vec | TS2Vec+S3 | DSN | DSN+S3 | InfoTS | InfoTS+S3 | SoftCLT | SoftCLT |
|-----------------------------|--------------|--------------|--------------|--------------|--------------|--------------|--------------|--------------|
| ArticulatoryWordRecognition | 0.987 | 0.983 | 0.980 | 0.993 | 0.983 | 0.993 | 0.993 | 0.997 |
| AtrialFibrillation | 0.200 | 0.400 | 0.267 | 0.533 | 0.266 | 0.400 | 0.200 | 0.400 |
| BasicMotions | 0.975 | 0.983 | 1.000 | 0.975 | 1.000 | 1.000 | 0.975 | 1.000 |
| CharacterTrajectories | 0.995 | 0.996 | 0.994 | 0.994 | 0.683 | 0.701 | 0.984 | 0.997 |
| Cricket | 0.986 | 1.000 | 0.986 | 0.944 | 0.958 | 0.986 | 0.972 | 0.986 |
| DuckDuckGeese | 0.500 | 0.500 | 0.620 | 0.660 | 0.560 | 0.580 | 0.500 | 0.420 |
| EigenWorms | 0.832 | 0.878 | 0.336 | 0.383 | 0.720 | 0.748 | 0.856 | 0.864 |
| Epilepsy | 0.964 | 0.964 | 1.000 | 0.884 | 0.957 | 1.000 | 0.935 | 0.971 |
| ERing | 0.874 | 0.848 | 0.907 | 0.956 | 0.926 | 0.944 | 0.911 | 0.937 |
| EthanolConcentration | 0.300 | 0.312 | 0.221 | 0.680 | 0.259 | 0.304 | 0.281 | 0.304 |
| FaceDetection | 0.498 | 0.516 | 0.638 | 0.652 | 0.525 | 0.564 | 0.534 | 0.534 |
| FingerMovements | 0.480 | 0.590 | 0.500 | 0.660 | 0.500 | 0.570 | 0.600 | 0.600 |
| HandMovementDirection | 0.270 | 0.338 | 0.297 | 0.649 | 0.408 | 0.541 | 0.419 | 0.486 |
| Handwriting | 0.519 | 0.476 | 0.353 | 0.306 | 0.529 | 0.534 | 0.493 | 0.480 |
| Heartbeat | 0.663 | 0.756 | 0.766 | 0.741 | 0.756 | 0.780 | 0.683 | 0.761 |
| InsectWingbeat | 0.466 | 0.437 | 0.322 | 0.483 | 0.466 | 0.469 | 0.485 | 0.478 |
| JapaneseVowels | 0.984 | 0.986 | 0.992 | 0.970 | 0.962 | 0.992 | 0.984 | 0.992 |
| Libras | 0.867 | 0.889 | 0.961 | 0.894 | 0.833 | 0.878 | 0.878 | 0.911 |
| LSST | 0.543 | 0.563 | 0.550 | 0.579 | 0.543 | 0.559 | 0.516 | 0.563 |
| MotorImagery | 0.510 | 0.540 | 0.490 | 0.640 | 0.580 | 0.610 | 0.530 | 0.560 |
| NATOPS | 0.922 | 0.956 | 0.961 | 0.983 | 0.928 | 0.950 | 0.967 | 0.983 |
| PEMS-SF | 0.694 | 0.723 | 0.786 | 0.861 | 0.740 | 0.844 | 0.682 | 0.746 |
| PenDigits | 0.990 | 0.989 | 0.987 | 0.982 | 0.983 | 0.987 | 0.987 | 0.988 |
| PhonemeSpectra | 0.240 | 0.240 | 0.315 | 0.114 | 0.233 | 0.282 | 0.223 | 0.231 |
| RacketSports | 0.855 | 0.868 | 0.868 | 0.865 | 0.895 | 0.914 | 0.862 | 0.855 |
| SelfRegulationSCP1 | 0.785 | 0.850 | 0.700 | 0.911 | 0.843 | 0.870 | 0.820 | 0.867 |
| SelfRegulationSCP2 | 0.578 | 0.578 | 0.506 | 0.583 | 0.567 | 0.606 | 0.494 | 0.589 |
| SpokenArabicDigits | 0.990 | 0.990 | 0.987 | 0.803 | 0.808 | 0.823 | 0.950 | 0.985 |
| StandWalkJump | 0.467 | 0.533 | 0.400 | 0.533 | 0.400 | 0.467 | 0.333 | 0.600 |
| UWaveGestureLibrary | 0.909 | 0.919 | 0.925 | 0.903 | 0.906 | 0.928 | 0.925 | 0.934 |
| Average | 0.695 | 0.720 | 0.687 | 0.737 | 0.691 | 0.727 | 0.699 | 0.734 |

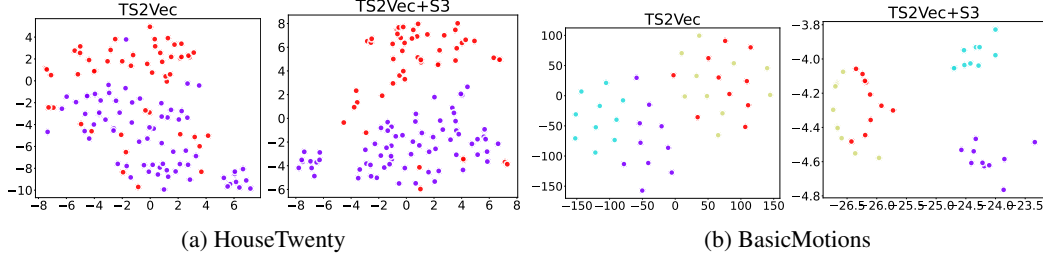


Figure A1: t-SNE visualizations of the learned representations for TS2Vec and TS2Vec+S3 for 2 randomly chosen test sets. Different colors represent different classes, where we observe better grouping of representations belonging to each class after the addition of S3.

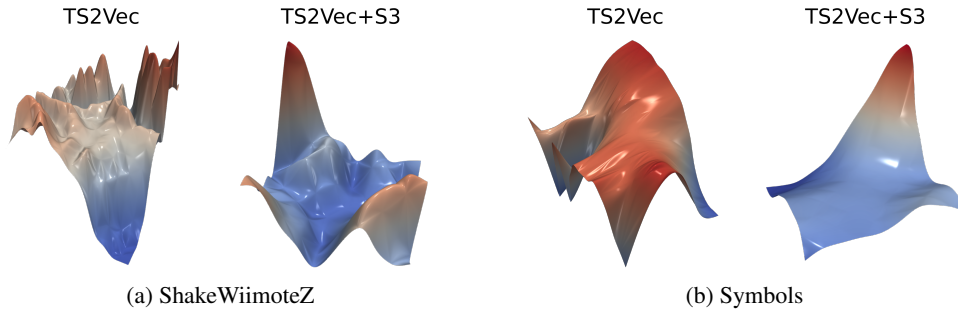


Figure A2: Visualisation of the loss landscape following [48], for TS2Vec and TS2Vec+S3 on two UCR datasets. It can be observed that the loss landscape with S3 is considerably smoother than the baseline without S3.

Table A3: Comparison of the measured standard deviation of the training loss for TS2Vec and TS2Vec+S3, over the first 75 UCR datasets.

| Dataset | TS2Vec | TS2Vec+S3 | Difference |
|--------------------------------|--------|-----------|---------------|
| ACSF1 | 2.39 | 1.56 | 34.65% |
| AllGestureWiimoteX | 1.19 | 0.88 | 26.38% |
| AllGestureWiimoteZ | 1.43 | 1.35 | 5.71% |
| BME | 23.59 | 21.24 | 10.00% |
| BirdChicken | 1.66 | 2.45 | -47.43% |
| CBF | 4.26 | 1.16 | 72.83% |
| ChlorineConcentration | 11.05 | 9.16 | 17.03% |
| Computers | 10.93 | 9.85 | 9.92% |
| CricketX | 2.82 | 1.51 | 46.49% |
| CricketY | 19.42 | 13.91 | 28.35% |
| CricketZ | 4.66 | 3.34 | 28.44% |
| DistalPhalanxOutlineAgeGroup | 13.17 | 0.92 | 93.00% |
| DistalPhalanxOutlineCorrect | 4.03 | 0.92 | 77.10% |
| DistalPhalanxTW | 4.32 | 0.95 | 77.98% |
| DodgerLoopWeekend | 557.35 | 798.64 | -43.29% |
| ECG200 | 1.85 | 1.67 | 9.64% |
| ECG5000 | 1.83 | 1.30 | 29.05% |
| EOGHorizontalSignal | 3.58 | 3.14 | 12.16% |
| EOGVerticalSignal | 2.83 | 1.66 | 41.09% |
| Earthquakes | 12.54 | 9.73 | 22.40% |
| EthanolLevel | 1.60 | 1.48 | 7.27% |
| FaceAll | 12.12 | 10.66 | 12.03% |
| FaceFour | 4.64 | 1.62 | 65.14% |
| FiftyWords | 5.10 | 4.47 | 12.31% |
| FordA | 2.94 | 2.55 | 13.13% |
| FordB | 1.41 | 1.31 | 7.24% |
| GestureMidAirD3 | 6.49 | 4.68 | 27.83% |
| HAR | 2.40 | 1.32 | 45.06% |
| Haptics | 1.42 | 1.06 | 25.90% |
| Herring | 2.60 | 2.64 | -1.77% |
| HouseTwenty | 9.22 | 8.35 | 9.38% |
| InlineSkate | 6.10 | 5.71 | 6.50% |
| InsectEPGRegularTrain | 11.61 | 4.14 | 64.37% |
| InsectEPGSmallTrain | 12.35 | 4.71 | 61.89% |
| ItalyPowerDemand | 13.87 | 0.86 | 93.83% |
| LargeKitchenAppliances | 13.10 | 7.66 | 41.51% |
| Lightning2 | 94.45 | 6.31 | 93.32% |
| Lightning7 | 2.13 | 1.37 | 35.46% |
| Meat | 4.75 | 4.31 | 9.19% |
| MedicalImages | 1.23 | 1.43 | -16.47% |
| MelbournePedestrian | 1.62 | 0.88 | 45.67% |
| MiddlePhalanxOutlineAgeGroup | 4.11 | 0.92 | 77.71% |
| MiddlePhalanxOutlineCorrect | 4.21 | 0.93 | 77.95% |
| MiddlePhalanxTW | 4.09 | 0.93 | 77.39% |
| MixedShapesRegularTrain | 2.48 | 2.38 | 4.17% |
| MixedShapesSmallTrain | 4.13 | 2.50 | 39.49% |
| MoteStrain | 8.07 | 0.98 | 87.92% |
| NonInvasiveFetalECGThorax1 | 2.75 | 2.48 | 9.83% |
| NonInvasiveFetalECGThorax2 | 3.20 | 2.80 | 12.73% |
| OSULeaf | 1.72 | 1.52 | 11.90% |
| OliveOil | 19.02 | 11.44 | 39.84% |
| PLAID | 4.67 | 2.98 | 36.09% |
| PhalangesOutlinesCorrect | 2.82 | 2.01 | 28.72% |
| Phoneme | 2.30 | 1.87 | 18.91% |
| PickupGestureWiimoteZ | 4.54 | 0.88 | 80.67% |
| PigAirwayPressure | 6.32 | 5.59 | 11.57% |
| PigArtPressure | 1.57 | 1.50 | 4.11% |
| PigCVP | 1.89 | 1.22 | 35.55% |
| Plane | 15.28 | 10.49 | 31.31% |
| PowerCons | 13.83 | 7.09 | 48.78% |
| ProximalPhalanxOutlineAgeGroup | 13.26 | 0.95 | 92.85% |
| ProximalPhalanxOutlineCorrect | 12.95 | 0.94 | 92.72% |
| ProximalPhalanxTW | 1.40 | 0.92 | 34.04% |
| RefrigerationDevices | 6.66 | 4.45 | 33.25% |
| Rock | 8.27 | 9.23 | -11.55% |
| ScreenType | 9.70 | 5.49 | 43.44% |
| SemgHandGenderCh2 | 9.78 | 7.59 | 22.44% |
| SemgHandMovementCh2 | 19.03 | 17.21 | 9.59% |
| SemgHandSubjectCh2 | 8.78 | 7.93 | 9.68% |
| ShakeGestureWiimoteZ | 2.41 | 0.83 | 65.65% |
| ShapeletSim | 3.32 | 1.12 | 66.18% |
| ShapesAll | 1.32 | 1.07 | 19.19% |
| SmallKitchenAppliances | 84.86 | 47.19 | 44.39% |
| SmoothSubspace | 1.58 | 0.85 | 46.46% |
| SonyAIBORobotSurface1 | 12.81 | 1.47 | 88.50% |
| Average | | | 34.69% |

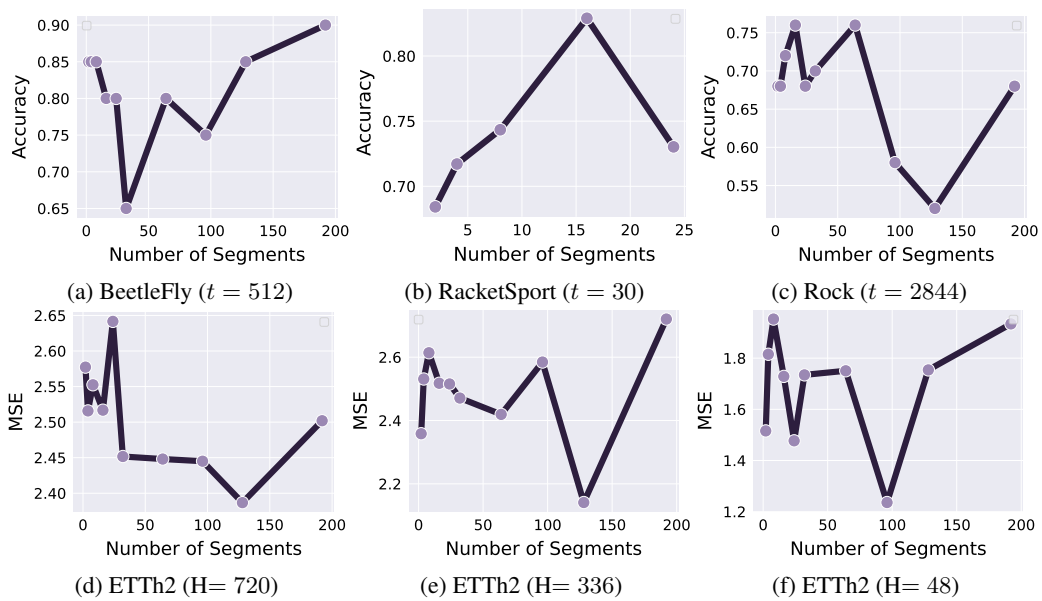


Figure A3: Performance vs. number of segment. In (a), (b), and (c), 3 UCR datasets for classification were used, and in (d), (e), and (f) the ETTh2 dataset for forecasting was used with 3 different horizon lengths. A higher value for accuracy is better, and a lower value MSE is better.